Degenerate Raman sideband cooling of ^{40}K atoms

Elad Zohar,* Yanay Florshaim,* Oded Zilberman, Amir Stern, and Yoav Sagi†
Physics Department and Solid State Institute, Technion – Israel Institute of Technology, Haifa 32000, Israel

(Received 10 August 2022; accepted 1 December 2022; published 23 December 2022)

We report on the implementation of degenerate Raman sideband cooling of ^{40}K atoms. The scheme incorporates a three-dimensional (3D) optical lattice, which confines the atoms and drives the Raman transitions. The optical cooling cycle is closed by two optical pumping beams. The wavelength of the laser beams forming the lattice is close to the D_2 atomic transition, while the optical pumping is operated near the D_1 transition. With this cooling method, we achieve a temperature of $\sim 1\,\mu$K of a cloud with $\sim 10^7$ atoms. This corresponds to a phase space density of $\geqslant 10^{-3}$. Moreover, the fermionic ensemble is spin polarized to conditions which are favorable for subsequent evaporative cooling. We study the dependence of the cooling scheme on several parameters, including the applied magnetic field and the detuning, duration, and intensity profile of the optical pumping beams. Adding this optical cooling stage to current Fermi gas experiments can improve the final conditions and increase the data rate.

DOI: 10.1103/PhysRevA.106.063111

I. INTRODUCTION

Ultracold atomic gases are used in a wide range of applications, from studying many-body physics [1–3], through quantum simulation and computation [4–7], and all the way to precision metrology [8–10]. Most such experiments require several cooling stages before the atoms can be used for the intended purpose. Laser cooling and evaporative cooling are the workhorses of this preparation procedure. The former has the advantage of being efficient, namely, being relatively fast and incurring only minor loss of atoms. A natural limitation of laser cooling is the recoil energy an atom acquires following an emission of a single photon. To mitigate this effect, the cooling rate has to be reduced as the cooling process progresses. One way to achieve this is to design the process such that atoms will accumulate in a low-energy final state which is almost decoupled from all the cooling lights. The buildup of population in this final dark state achieves another desirable goal: spin polarization. The alternative route to preparing a sample in a well-defined internal state is by optical pumping, but it leads to heating due to spontaneous photon scattering. A cooling scheme that ends with all atoms being in a single dark state at a very low temperature solves this problem.

One of the most successful and widely used methods to approach and go below the recoil limit is to employ Raman transitions. Originally, the technique was developed in continuous space [11], with a series of velocity-selective Raman pulses. The technique was then adopted to a single trapped ion [12] and atoms in an optical lattice [13,14]. This approach is called Raman sideband cooling (RSC) since the two Raman photons drive transitions $n \to n-1$, where n is the vibrational state in any given lattice site. Since the transition induced by a continuous Raman process is reversible, it cannot by itself lead to cooling. To break time-reversal symmetry, one can either make the Hamiltonian time dependent (e.g., pulsing the Raman beams [11]) or introduce a dissipative irreversible process, such as spontaneous emission. In the case of Raman cooling in an optical lattice, the latter is achieved by optical pumping. In the Lamb-Dicke regime, the spontaneous emission is not likely to change the vibrational state. Thus, the cooling cycle is closed with some of the vibrational energy removed.

A particularly clever implementation of Raman sideband cooling uses the lattice light itself to drive the Raman transitions [15]. That means that the transition $n \to n-1$ needs to be degenerate, since the two Raman photons have the same frequency. Degenerate Raman sideband cooling (dRSC) was first realized with Cs atoms in a one-dimensional (1D) geometry [15], and later extended to three dimensions [16,17]. It achieved atomic densities that approach the lattice site density and a temperature of $1.5T_{\mathrm{rec}}$, where $T_{\mathrm{rec}} = \hbar^2 k^2/mk_B$ is the recoil temperature. dRSC was successfully implemented with the bosonic isotopes ^{87}Rb [18,19], ^{85}Rb [20], and ^{39}K [21]. To the best of our knowledge, dRSC was not implemented with fermionic atoms. Here, we report on a realization of dRSC with the fermionic isotope of potassium (^{40}K). Nondegenerate RSC was previously used to image single ^{40}K atoms in an optical lattice [22]. In our implementation, we start with a nondegenerate gas and optimize the scheme to achieve the highest phase space density and prepare the gas for further cooling. Although Pauli blocking could potentially harm dRSC for fermions, we observe results comparable to those in similar experiments with bosons.

Our complete cooling sequence begins with loading a three-dimensional (3D) magneto-optical trap (MOT) with approximately 10^7 atoms, followed by gray molasses cooling (GMC) [23,24] on the D_1 line. The GMC stage cools the atoms to $\sim 5\,\mu$K, while leaving them occupying all spin states

*These authors contributed equally to this work.
†yoavsagi@technion.ac.il

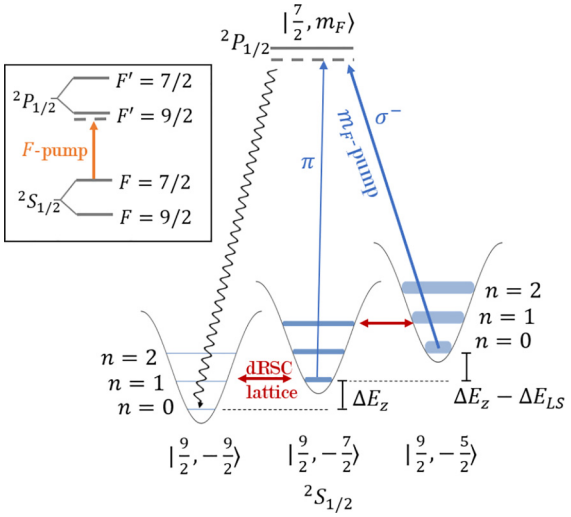

FIG. 1. Degenerate Raman sideband cooling scheme with ^{40}K atoms. The lattice provides the confining potential (here depicted for a single lattice site), as well as drives Raman transitions (depicted by red horizontal arrows) between the different m_F states of the $F = 9/2$ ground state level with different vibrational principle numbers n. The energy of different m_F states with the same n is shifted due to the applied magnetic field. Necessary components in the cooling cycle are the m_F and F optical pumping beams. The former pumps atoms in the $F = 9/2$ towards negative spin states, while the latter brings back into the cooling cycle atoms that decay to the $F = 7/2$ level. The m_F pump carries a strong σ^- polarization component and a weak π component. This leads to broadening of the $m_F \geqslant -5/2$ states (depicted by a larger width of the n levels), as well as creates a differential light shift, ΔE_{LS}, which for red detuning shifts the $m_F = -5/2, -7/2$ to lower energies. The wavelengths of the Raman and optical pumping lasers are close to the D_2 and D_1 lines, respectively.

of the $F = 9/2$ ground state manifold. Then, we load the cloud into the Raman optical lattice, and within a few milliseconds of dRSC we achieve a spin polarized sample with a temperature as low as $1\,\mu$K, which is around $1.2T_{\mathrm{rec}}$. The highest phase space density (PSD) we measure is around 10^{-3}, two orders of magnitude higher than that of the cloud immediately after the GMC stage. The dRSC leaves over 80% of the atoms in the $F = 9/2, m_F = -9/2$ ground state, and the rest are at $m_F = -7/2$ (see Fig. 1). These conditions significantly improve the starting point and efficiency of subsequent forced evaporation, which we perform in a crossed far-off-resonance dipole trap. Since identical ultracold fermions cannot interact through symmetric s-wave scattering, the remaining 20% of the atoms in the $m_F = -7/2$ state are essential for fast thermalization and efficient evaporation [25,26]. Moreover, a mixture of these two spin states is a natural choice for quantum simulation experiments since they are stable against spin-exchange collisions and offer a convenient Feshbach resonance around 202.14G [27], which allows tuning the strength of their interaction [28]. It is also possible to change the spin composition by driving spin rotations with a radio-frequency radiation that matches the energy difference between the two spin states [29].

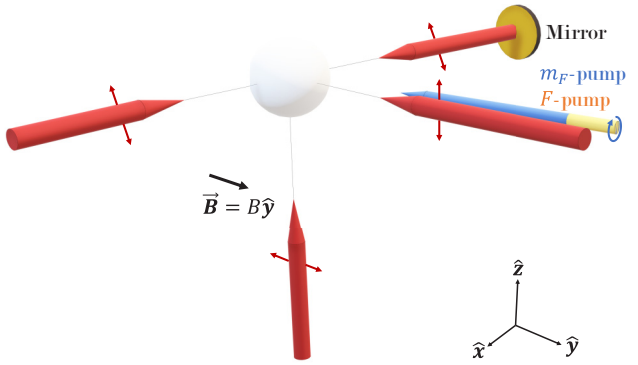

FIG. 2. Schematic of the optical and magnetic setup of the dRSC scheme. The lattice is formed by four beams (thick red arrows). The two beams along the $\hat{x}$ direction are created by a single retro-reflected beam. The other two beams cross at an angle very close to 90°. The polarization of all lattice beams (depicted as thin arrows) lie in the y-z plane. The magnetic field $\vec{B}$ is directed along the $\hat{y}$ direction. The circularly polarized m_F-pump and F-pump beams (blue and yellow arrow) propagate at an angle of approximately 5° relative to the magnetic field, chosen to introduce a small π polarization component required to complete the cooling cycle.

II. EXPERIMENT

A sketch of the experimental setup is presented in Fig. 2. The 3D lattice is created by four beams: one beam, propagating along the x axis in the sketch, is retro-reflected, while the two others, propagating along the y and z axes, are free running. All beams are linearly polarized; the retro-reflected beam is polarized at an angle of 45° relative to the z axis, as depicted in Fig. 2. This makes the dipole potential induced by the lattice isotropic in two out of three axes (y and z). All polarizations of the lattice beams, as well as the magnetic field, lie in the same y-z plane.

The source of the lattice beams is a distributed Bragg reflector (DBR) laser, whose frequency is red detuned -11 GHz with respect to the D_2 line. By deriving all lattice beams from the same source, we ensure that relative phase shifts do not modify the lattice geometry but only translate the entire lattice, which does not harm the cooling process [21,30]. The lattice laser is amplified by a home-built tapered amplifier (TA) and then passed through an acousto-optic modulator (AOM) for fast intensity control. It is also passed through a temperature stabilized solid etalon to filter out the broadband amplified spontaneous emission (ASE). The etalon has a free spectral range (FSR) of 60 GHz and a bandwidth of 1.6 GHz.

After the etalon, we split the light once using a $\lambda/2$ plate and a polarizing beam splitter (PBS), and then a second time using a nonpolarizing beam splitter (NPBS). The $\lambda/2$ plate allows us control over the ratio between the power of the retro-reflected beam ($\hat{x}$) and the $\hat{y}$ and $\hat{z}$ beams, which is typically set such that the former has twice the power of the latter. This ratio was optimized experimentally at a fixed lattice detuning. All beams are then sent to the experiment via three 5-m single-mode polarization maintaining optical fibers. We sample and monitor the power of one of the beams with a photodiode at the fiber output, and then use a servo loop and the AOM before the fibers to stabilize it. The total power of all

three beams is kept at 100 mW, which yields a peak intensity of 1590 mW/cm^2 (795 mW/cm^2) and thus a calculated depth of 586 μK (238 μK) in the $\hat{x}$ ($\hat{y}$ and $\hat{z}$) direction. With these parameters, the calculated harmonic trapping frequencies in each of the lattice sites are 344 kHz in the $\hat{x}$ direction and 138 kHz in the $\hat{y}$, $\hat{z}$ directions. The magnetic field is applied using two pairs of external Helmholtz coils, such that the total field points in the desired direction.

There are two optical pumping beams in our setup: the m_F pump and F pump. The m_F pump is set as close as possible to perfect circular polarization. Due to a small angle between it and the magnetic field, it carries a strong (weak) σ^- (π) component. The strong σ^- component pumps the atoms from the $|F = \frac{9}{2}, m_F\rangle$ states to the $|F' = \frac{7}{2}, m_F - 1\rangle$ states of the excited $P_{1/2}$ level, after which they spontaneously decay predominantly to the $|F = \frac{9}{2}, m_F - 1\rangle$ state (see Fig. 1). Because the entire process is performed in the Lamb-Dicke regime, that is, the Lamb-Dicke parameter $\eta = \sqrt{\frac{E_R}{\hbar\omega_{\text{lattice}}}} = 0.31$ (0.49) for the $\hat{x}$ ($\hat{y}$ and $\hat{z}$) direction (E_R is the photon recoil energy), this process is unlikely to change the vibrational state of the atom. This means that atoms undergo several cycles which consist of a Raman transition that lowers the vibrational state and an m_F pump which resets the atoms to the $m_F = -7/2$, until they reach the ground state. The weak π component is used to pump the atoms to $m_F = -9/2$, at which point they are decoupled from both the Raman and optical pumping processes. Note that η cannot be too small because it reduces the Raman transition rate. The second optical pumping beam (F pump) is used to pump atoms which decay from the m_F-pumping process to the $F = 7/2$ ground state manifold, which is not part of the cooling process. The F pumping is performed through the $F = 9/2$ state of the D_1 level. We send both optical pumping lights through the same optical fiber. The m_F pump is locked to the D_1 line using a saturated absorption spectroscopy (SAS) setup [31], and the F-pump frequency is stabilized relative to the m_F pump by monitoring their beat signal [32]. The required frequency shifts which bring each of the optical pumping lights to the desired detunings are achieved using several AOMs.

The full loading sequence is thus as follows. ^{40}K atoms are dispensed from home-built dispensers, then trapped and cooled in a two-dimensional (2D) MOT [33,34] and pushed into the main vacuum chamber. There, a 3D MOT captures and cools them further during 6 s of loading time. Following the 3D MOT, the atoms are cooled for 8 ms with a gray molasses D_1 cooling scheme [23,24], during which the magnetic field is set to zero using three pairs of Helmholtz coils. We then turn off the D_1 cooling light and simultaneously ramp up in 0.8 ms the Raman lattice power and the magnetic field. The magnetic field is ramped to 500 mG using two of the three Helmholtz coils, such that it points in the desired direction, as depicted in Fig. 2. With the lattice and magnetic fields ready, we turn on the m_F-pump and F-pump beams. During optimization, we found that optimal cooling is achieved when the m_F pump is linearly ramped up from a low initial intensity of 0.1 mW/cm^2 to 2.1 mW/cm^2 during the 10 ms of dRSC. We discuss this observation in the Results section.

After 10 ms of cooling, we turn off the optical pumping lights and ramp down the lattice for another 0.8 ms. In future experiments, the next step in the sequence would require the atoms to be loaded into a crossed dipole trap. We therefore studied the optimal loading sequence and found no significant difference in cooling efficiency if the crossed trap is kept on during the GMC and dRSC processes. Once the Raman lattice is ramped down, we capture in the crossed dipole trap more than 10^6 atoms (12% of the atoms in the dRSC) at the same phase space density as without a trap. Since the presence of the crossed trap compresses the atoms in real space, the temperature immediately after their loading is 7 μK. However, apart from the spin composition measurement, all the results presented below were taken without the crossed dipole trap, therefore they give a faithful characterization of only the dRSC process.

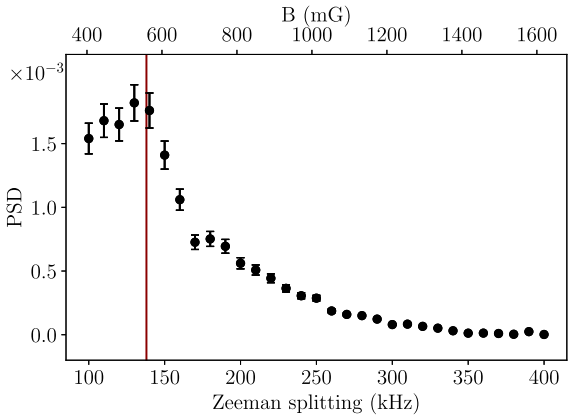

FIG. 3. The final phase space density as a function of the applied magnetic field. The upper x axis provides the actual field magnitude, while the bottom x axis gives the Zeeman splitting between the $|9/2, -9/2\rangle$ and $|9/2, -7/2\rangle$ states associated with this field. Since we are working in the linear regime of the Zeeman splitting, other m_F levels would be shifted approximately (up to a few hertz) by the same amount. The vertical red line marks the harmonic trapping frequency in the $\hat{y}$, $\hat{z}$ directions. Error bars in this paper represent one standard deviation.

III. RESULTS

To characterize the gas conditions, we measure the integrated density distribution of the cloud using absorption imaging, both *in situ* and after a time-of-flight of typically 30 ms. We fit the distributions measured at the two times with a Gaussian, and from the change in their widths we extract the cloud temperature. In addition, integration over the density gives us the total number of atoms. We can then calculate the PSD given by $n\lambda_{\text{dB}}^3$, where n is the density and λ_{dB} is the thermal de Broglie wavelength. We use the number of atoms, and the volume as approximated by a Gaussian sphere of a radius $\frac{\sigma_x+\sigma_y}{2}$, where σ_i is the *in situ* Gaussian width in direction i, to calculate n.

We now turn to characterize the dependence of the cooling sequence on various parameters. First, we calibrate the optimal magnetic field magnitude required for cooling. To this end, we fix all other parameters, scan the magnetic field, and extract the PSD. As can be seen in Fig. 3, the optimum fits the theoretical lattice frequency in the two isotropic directions.

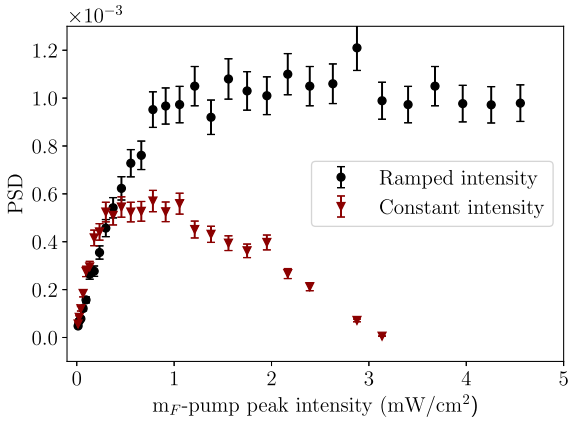

FIG. 4. Phase space density for different m_F-pump intensities. Runs with constant (ramped) pump intensity are marked by triangles (circles). In the ramped intensity experiments, the x axis gives the final m_F-pump intensity after a linear ramp from an initial intensity of $0.1\,\mathrm{mW/cm^2}$. We attribute the improvement when ramping the intensity to a smooth change of the light shift induced by the m_F pump, which compensates for the inhomogeneous anharmonic broadening of the transition frequencies in the lattice.

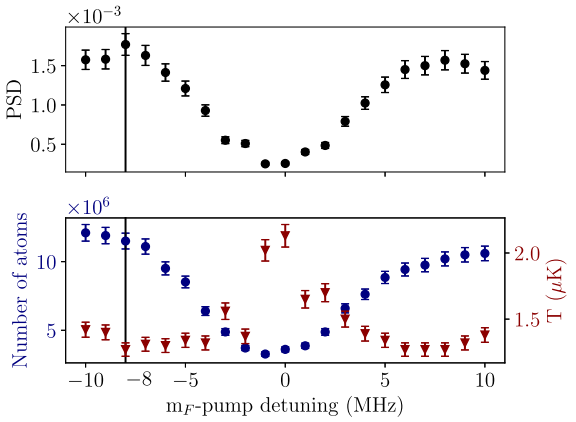

FIG. 5. Upper panel: Phase space density after applying dRSC with different m_F-pump detuning. It exhibits a slightly better performance on the red side. Lower panel: Number of atoms (blue circles, left axis) and temperature (red triangles, right axis) from which the PSD was calculated. The chosen working condition is marked by a vertical black line.

There is no distinct peak corresponding to the trapping frequency in the $\hat{x}$ direction because the Raman coupling in that direction is vanishingly small due to the standing wave [15]. The cooling, however, is still three dimensional, probably due to mixing between the axes in an imperfect lattice potential, as well as diffusion effects.

The second parameter we scan to optimize the dRSC is the m_F-pump intensity, with the detuning fixed at $-8\,\mathrm{MHz}$. We have tested two different intensity time profiles, constant and linear, and the results are presented in Fig. 4. When the intensity is constant in time, we observe that the PSD is higher for a larger intensity, until it saturates around 0.5×10^{-3} for an intensity of $\sim 0.5\,\mathrm{mW/cm^2}$. At even higher intensity, the PSD decreases. We attribute this behavior to the interplay between the Raman and optical pumping transition rates. The calculated Raman Rabi frequency is $\Omega_R/2\pi \approx 70$ kHz. The optical pumping rate is much faster than this frequency, which means that the atoms are quickly pumped into the dark states described above. However, in the experiment the polarization of the optical pumping beam cannot be perfectly σ^-. The undesired σ^+ component pumps out atoms from the dark states, which leads to heating. We estimate that 0.1% of the light is in the σ^+ polarization, which yields a Rabi frequency on the order of Ω_R. As a result, transitions that increase the vibrational quantum number become too frequent, and atoms eventually become untrapped and leave the lattice.

Instead, we find that it is beneficial to initiate the optical pumping at low intensity ($0.1\,\mathrm{mW/cm^2}$) and then ramp it linearly to a higher value. Results following this procedure are shown in Fig. 4 versus the final intensity. With ramping we obtain a twofold improvement in the final PSD. There are two plausible explanations for this effect. First, there is a higher efficiency of the optical pumping with the π component at the final stages of the cooling process. Second, the linear ramp induces a smooth change of the light shift (ΔE_{LS} in Fig. 1), which is better suited to the nonuniform and anharmonic lattice potential. In what follows, we fix the intensity profile of the m_F pump to linear ramping with a final intensity of $2.1\,\mathrm{mW/cm^2}$.

Next, we study the dependence of the cooling process on the m_F-pump detuning (Fig. 5). Previous implementations of dRSC with other atomic species found that it is advantageous to work with a blue detuned m_F pump [16,21]. In contrast, we observe that the dependence is almost symmetric with respect to the sign of the detuning, with slightly better results obtained when working with a red detuned light. As for the F pump, we find that the detuning and power do not affect the final temperature, or increase the loss, as long as the intensity is above $4\,\mathrm{mW/cm^2}$ and the detuning is at least $-4\,\mathrm{MHz}$. This behavior is in line with previous results obtained with ^{39}K [21].

One of the advantages of dRSC is its ability to spin polarize the ensemble. To determine the final spin composition, we perform microwave (MW) spectroscopy after the cooling process is done. First, we load the atoms from the lattice to a crossed optical dipole trap. Then, we apply a MW field whose frequency we ramp over 50 kHz to compensate for magnetic field fluctuations. The MW field drives a $|F = \frac{9}{2}, m_F\rangle \rightarrow |F = \frac{7}{2}, m_F'\rangle$ transition in the ground state manifold. The MW central frequency determines which m_F, m_F' levels we address, based on the Zeeman splitting. Then, we turn on a quadruple magnetic field which traps only the atoms transferred by the MW pulse while the other atoms are ejected out [27]. Finally, we detect the atoms captured in the quadruple trap using MOT fluorescence. The inset of Fig. 6 shows an example of this spectroscopy, from which we extract the relative population in each state. In the main graph of Fig. 6 we present the spin composition for different durations of the dRSC. One can see that after a few milliseconds, over 95% of the atoms occupy the two $m_F = -9/2, -7/2$ states. In about 10 ms, their fraction saturate towards 80% and 20%, respectively. In an ideal dRSC, the $m_F = -9/2$ population should ultimately approach unity. In practice, off-resonant excitations to the $F' = 9/2$ state,

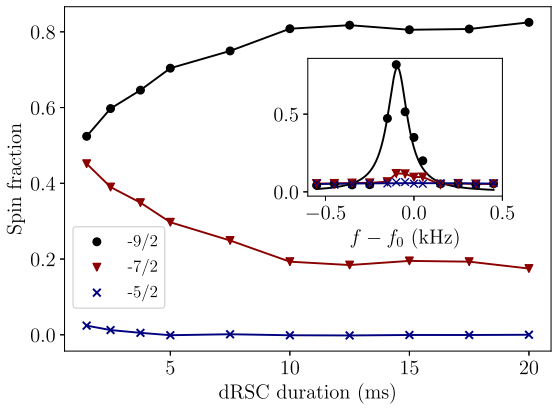

FIG. 6. Fraction of different m_F states vs the duration of the dRSC sequence. Atoms are quickly pumped to occupy the two lowest m_F states, after which the small π component of the m_F pump continues to reduce the population in the $m_F = -7/2$ state. The inset shows an example of the spectrum from which the fractions are extracted, where all three resonance frequencies of the different m_F states are centered around the bare transition resonance f_0, which depends on m_F and the magnetic field. The spectrum is fitted with a Lorentzian to find the spectral weight.

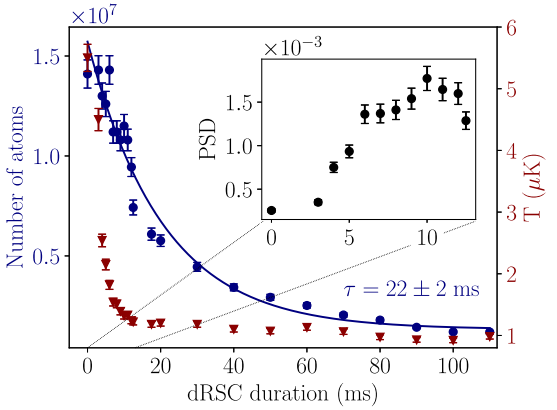

FIG. 7. Number of atoms (circles, left axis) and temperature (triangles, right axis) as a function of the duration of the dRSC. For measurements shorter than or equal to 10 ms, the intensity of the m_F pump is linearly ramped between the same initial and final values during the dRSC duration. For longer times we keep all lights at their final intensity from 10 ms and on. The number of atoms is fitted with an exponential decay, yielding $\tau = 22 \pm 2$ ms. The inset shows a close-up of the phase space density in the first 12 ms. The point at zero time represents the conditions after the GMC. The asymptotic temperature we observe after 10 ms of cooling is $\sim$1 μK, and at this point the PSD peaks at $\sim 1.5 \times 10^{-3}$.

imperfect polarization of the m_F pump, and single photon scattering from the Raman lattice beams contribute to the observed asymptotic spin composition.

Finally, we measure the lifetime of the atoms in the lattice. This measurement is done in the following way: The first 10 ms are performed in the same manner as described before, including ramping the m_F pump. For longer durations, we keep all lights and the magnetic field at a fixed value after the initial 10 ms. The resulting number of atoms and temperature versus the total duration are shown in Fig. 7. The inset shows the PSD in the first 12 ms. Based on this measurement, we choose the cooling time to be 10 ms. We fit the number of atoms data with an exponentially decaying function and find a timescale of $\tau = 22 \pm 2$ ms, much shorter than the vacuum limited lifetime of 6.5 ± 0.5 s. Since the cooling achieves optimal conditions in 10 ms, this lifetime does not harm the usefulness of the dRSC technique. We attribute the loss to the spatial Gaussian profile of the lattice beams, which gives rise to a spatially varying lattice depth and harmonic trapping frequency. Specifically, the lattice beams' waist radius is around 1 mm, while the atomic cloud radius is around 0.5 mm. This means that in the outer regions of the lattice the Raman degeneracy condition is not met and atoms are heated and lost. In addition, we measure the heating rate in the lattice without any optical pumping light to be $\sim$4 μK/ms. This rate is of the same order as the cooling rate. The loss rate could be reduced by increasing the lattice detuning and working with larger lattice beams. Both of these solutions, however, require considerably more laser power than what we currently have at hand.

IV. SUMMARY AND OUTLOOK

We have presented an experimental implementation of dRSC with the fermionic isotope of potassium ^{40}K. The cooling scheme achieves a fivefold reduction in temperature, compared to gray molasses cooling, and concurrently spin polarizes the sample. By ramping up the m_F-pump light intensity, we achieve a twofold improvement in phase space densities achieved by this scheme when compared to using a constant intensity. The dRSC scheme greatly improves the loading conditions to a crossed dipole trap for subsequent evaporative cooling. Our implementation employs an optical lattice close to the D_2 line and optical pumping beams red detuned relative to the D_1 line. In the future, this separation of wavelengths can allow sensitive detection of the atoms' position using the dRSC scheme and filtering out efficiently unwanted D_2 light scattering.

ACKNOWLEDGMENTS

This research was supported by the Israel Science Foundation (ISF), Grants No. 3491/21 and No. 1779/19, and by the Pazy Research Foundation.

[1] I. Bloch, J. Dalibard, and W. Zwerger, Many-body physics with ultracold gases, Rev. Mod. Phys. **80**, 885 (2008).
[2] C. Noh and D. G. Angelakis, Quantum simulations and many-body physics with light, Rep. Prog. Phys. **80**, 016401 (2017).
[3] A. Browaeys and T. Lahaye, Many-body physics with individually controlled Rydberg atoms, Nat. Phys. **16**, 132 (2020).
[4] A. D. Ludlow, M. M. Boyd, J. Ye, E. Peik, and P. O. Schmidt, Optical atomic clocks, Rev. Mod. Phys. **87**, 637 (2015).

[5] M. Endres, H. Bernien, A. Keesling, H. Levine, E. R. Anschuetz, A. Krajenbrink, C. Senko, V. Vuletic, M. Greiner, and M. D. Lukin, Atom-by-atom assembly of defect-free one-dimensional cold atom arrays, Science **354**, 1024 (2016).

[6] A. Cooper, J. P. Covey, I. S. Madjarov, S. G. Porsev, M. S. Safronova, and M. Endres, Alkaline-Earth Atoms in Optical Tweezers, Phys. Rev. X **8**, 041055 (2018).

[7] Y. Wang, S. Shevate, T. M. Wintermantel, M. Morgado, G. Lochead, and S. Whitlock, Preparation of hundreds of microscopic atomic ensembles in optical tweezer arrays, npj Quantum Inf. **6**, 54 (2020).

[8] A. D. Cronin, J. Schmiedmayer, and D. E. Pritchard, Optics and interferometry with atoms and molecules, Rev. Mod. Phys. **81**, 1051 (2009).

[9] X. Zhang and J. Ye, Precision measurement and frequency metrology with ultracold atoms, Natl. Sci. Rev. **3**, 189 (2016).

[10] X. Wu, Z. Pagel, B. S. Malek, T. H. Nguyen, F. Zi, D. S. Scheirer, and H. Müller, Gravity surveys using a mobile atom interferometer, Sci. Adv. **5**, eaax0800 (2019).

[11] M. Kasevich and S. Chu, Laser Cooling Below a Photon Recoil with Three-Level Atoms, Phys. Rev. Lett. **69**, 1741 (1992).

[12] C. Monroe, D. M. Meekhof, B. E. King, S. R. Jefferts, W. M. Itano, D. J. Wineland, and P. Gould, Resolved-Sideband Raman Cooling of a Bound Atom to the 3D Zero-Point Energy, Phys. Rev. Lett. **75**, 4011 (1995).

[13] S. E. Hamann, D. L. Haycock, G. Klose, P. H. Pax, I. H. Deutsch, and P. S. Jessen, Resolved-Sideband Raman Cooling to the Ground State of an Optical Lattice, Phys. Rev. Lett. **80**, 4149 (1998).

[14] H. Perrin, A. Kuhn, I. Bouchoule, and C. Salomon, Sideband cooling of neutral atoms in a far-detuned optical lattice, Europhys. Lett. **42**, 395 (1998).

[15] V. Vuletić, C. Chin, A. J. Kerman, and S. Chu, Degenerate Raman Sideband Cooling of Trapped Cesium Atoms at Very High Atomic Densities, Phys. Rev. Lett. **81**, 5768 (1998).

[16] A. J. Kerman, V. Vuletić, C. Chin, and S. Chu, Beyond Optical Molasses: 3D Raman Sideband Cooling of Atomic Cesium to High Phase-Space Density, Phys. Rev. Lett. **84**, 439 (2000).

[17] D.-J. Han, S. Wolf, S. Oliver, C. McCormick, M. T. DePue, and D. S. Weiss, 3D Raman Sideband Cooling of Cesium Atoms at High Density, Phys. Rev. Lett. **85**, 724 (2000).

[18] J. Hu, A. Urvoy, Z. Vendeiro, V. Crépel, W. Chen, and V. Vuletić, Creation of a Bose-condensed gas of ^{87}Rb by laser cooling, Science **358**, 1078 (2017).

[19] A. Urvoy, Z. Vendeiro, J. Ramette, A. Adiyatullin, and V. Vuletić, Direct Laser Cooling to Bose-Einstein Condensation in a Dipole Trap, Phys. Rev. Lett. **122**, 203202 (2019).

[20] C. Huang, P.-C. Kuan, and S.-Y. Lan, Laser cooling of ^{85}Rb atoms to the recoil-temperature limit, Phys. Rev. A **97**, 023403 (2018).

[21] M. Gröbner, P. Weinmann, E. Kirilov, and H.-C. Nägerl, Degenerate Raman sideband cooling of ^{39}K, Phys. Rev. A **95**, 033412 (2017).

[22] L. W. Cheuk, M. A. Nichols, M. Okan, T. Gersdorf, V. V. Ramasesh, W. S. Bakr, T. Lompe, and M. W. Zwierlein, Quantum-Gas Microscope for Fermionic Atoms, Phys. Rev. Lett. **114**, 193001 (2015).

[23] G. Salomon, L. Fouché, P. Wang, A. Aspect, P. Bouyer, and T. Bourdel, Gray-molasses cooling of ^{39}K to a high phase-space density, Europhys. Lett. **104**, 63002 (2013).

[24] D. R. Fernandes, F. Sievers, N. Kretzschmar, S. Wu, C. Salomon, and F. Chevy, Sub-doppler laser cooling of fermionic ^{40}K atoms in three-dimensional gray optical molasses, Europhys. Lett. **100**, 63001 (2012).

[25] B. DeMarco and D. S. Jin, Onset of Fermi degeneracy in a trapped atomic gas, Science **285**, 1703 (1999).

[26] W. Geist and T. A. B. Kennedy, Evaporative cooling of mixed atomic fermions, Phys. Rev. A **65**, 063617 (2002).

[27] C. Shkedrov, Y. Florshaim, G. Ness, A. Gandman, and Y. Sagi, High-Sensitivity rf Spectroscopy of a Strongly Interacting Fermi Gas, Phys. Rev. Lett. **121**, 093402 (2018).

[28] J. L. Bohn, Cooper pairing in ultracold ^{40}K using Feshbach resonances, Phys. Rev. A **61**, 053409 (2000).

[29] C. Shkedrov, M. Menashes, G. Ness, A. Vainbaum, E. Altman, and Y. Sagi, Absence of Heating in a Uniform Fermi Gas Created by Periodic Driving, Phys. Rev. X **12**, 011041 (2022).

[30] G. Grynberg, B. Lounis, P. Verkerk, J.-Y. Courtois, and C. Salomon, Quantized Motion of Cold Cesium Atoms in Two- and Three-Dimensional Optical Potentials, Phys. Rev. Lett. **70**, 2249 (1993).

[31] M. Kroll, Hyperfine Structure in the Visible Molecular-Iodine Absorption Spectrum, Phys. Rev. Lett. **23**, 631 (1969).

[32] U. Schünemann, H. Engler, R. Grimm, M. Weidemüller, and M. Zielonkowski, Simple scheme for tunable frequency offset locking of two lasers, Rev. Sci. Instrum. **70**, 242 (1999).

[33] S. Bhushan and R. K. Easwaran, Theoretical design for generation of slow light in a two-dimensional magneto optical trap using electromagnetically induced transparency, Appl. Opt. **56**, 3817 (2017).

[34] J. Nellessen, J. Werner, and W. Ertmer, Magneto-optical compression of a monoenergetic sodium atomic beam, Opt. Commun. **78**, 300 (1990).